JOURNAL OF MATERIALS SCIENCE **39** (2004) 5915–5924

The hypersonic environment: Required operating conditions and design challenges

D. M. VAN WIE, D. G. DREWRY JR., D. E. KING, C. M. HUDSON
The Johns Hopkins University, Applied Physics Laboratory, Laurel, Maryland, 20723-6099, USA
E-mail: Dave.VanWie@jhuapl.edu

Hypersonic flight powered by airbreathing engines offers the potential for faster response time at long ranges, and reduced cost for access-to-space. In the present paper the operating environment of typical hypersonic vehicles are discussed, including results for the radiation equilibrium wall temperature of external vehicle surfaces and the flow properties through three sample engines spanning the range of hydrocarbon-fueled Mach 4-8 flight and hydrogen-fueled flight at speeds up to Mach 17. Flow conditions at several locations through the sample engines were calculated to provide indications of the required operating flow environment. Additional system consideration such a seals, joints, vehicle integration and in-service engineering are addressed.

1. Introduction

The recent resurgence of interest in hypersonic systems can be traced to the desire for higher-speed interceptor missiles, long-range fast-response strike weapons and an affordable access-to-space transportation system. In attempting to define the term "hypersonics," many classical aerodynamicists attempt to draw a distinction between supersonic and hypersonic vehicles by referring to hypersonic effects such as Mach number independence, chemically reacting airflows, and highly cooled boundary layers. Each of these phenomena becomes more prevalent as flight speed increases, but step changes in their importance do not occur, so the definition of hypersonic is somewhat blurred. Within this paper, the term "hypersonic" will be used to refer to vehicles that operate at speeds greater than Mach 5. These vehicles fall into the following categories: ballistic missiles, re-entry vehicles, space access vehicles, interceptor missiles, hypersonic cruise missiles, and hypersonic cruise aircraft, which can be easily divided into single-use expendable and reusable systems.

While material and structural solutions for ballistic missiles, re-entry vehicles, and rocket-powered space access vehicles have been highly developed, system requirements are driving material operating temperatures to higher levels for interceptor missiles, hypersonic cruise missiles and aircraft, and space-access vehicles powered by airbreathing engines. For example, conventional material solutions include: Reinforced Carbon-Carbon (RCC) leading edges, silica-based High Temperature Reusable Surface Insulation (HTRSI) and Fibrous Refractory Composite Insulation (FRCI) tiles over aluminum substructure for the Space Shuttle; ablative phenolic resins within metallic honeycomb substrates, pyrolytic graphite and 3-D woven graphite fiber composites for re-entry vehicles; and fused silica, Pyroceram 9606 or silicon nitride for interceptor radomes.

In the present paper, the operating conditions for hypersonic vehicles will be explored together with a discussion of the typical design issues encountered in vehicle development. The principal emphasis will be on vehicles powered by airbreathing propulsion systems, since these systems are the most immature at the present time. These vehicles typically fly in a relatively narrow Mach number/altitude corridor corresponding to flight dynamic pressures, q, between 0.24 and 0.95 atm. By providing higher temperature materials, uncooled surfaces can be operated at higher speeds, and a better thermal match can be achieved for cooled surfaces between the fuel required for cooling the vehicle and fuel required to operate the engine.

As illustrated in Fig. 1, the dominant feature of these hypersonic vehicles is the engine, which consists of an inlet, isolator, combustor and nozzle. The material requirements for each component vary with flight condition, whether or not the surfaces are actively cooled, and whether the intended mission requires an expendable or reusable vehicle. Aspects of the individual component requirements will be addressed in the following sections. To assess the operating conditions, three sample dual-mode scramjet engines were designed with the characteristics provided in Table I. The first engine was designed for Mach 6 operation using JP-7 fuel with operating conditions explored at speeds between Mach 4 and 8. The second engine was designed for Mach 10 operation using hydrogen fuel, with operating conditions explored at speeds between Mach 6 and 14. The final engine was designed for operation at Mach 15 with engine operation explored at speeds between mach 10 and 17. Conditions through the engines were calculated using an engine cycle analysis tool that assumes equilibrium chemistry.

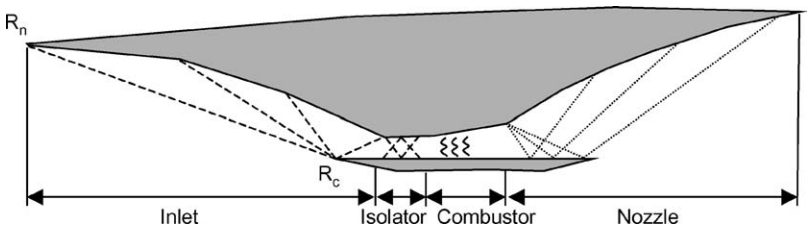

Figure 1 Generic hypersonic vehicle powered by dual-mode scramjet.

2. Component operating requirements

2.1. Stagnation regions

Vehicle performance and engine operating conditions dictate that the leading edges of hypersonic vehicles are relatively sharp, so the stagnation regions at the vehicle leading edge and cowl lip represent zones of high aerodynamics heating rates. Following the theory of Fay and Ridell [1–4], the heating rate to the wall, $\dot{q}_w$, at a spherical leading edge for boundary layers in chemical equilibrium can be expressed as:

$$\dot{q}_w = 0.76 Pr^{-0.6} (\rho_e \mu_e)^{0.4} (\rho_w \mu_w)^{0.1} \times \sqrt{\frac{dU_e}{dx}} (h_{te} - h_w) \left[1 - (Le^{0.51} - 1) \frac{h_D}{h_{te}} \right] \quad (1)$$

where Pr, Prandtl number; ρ, density; μ, viscosity; h, enthalpy; Le, Lewis number, and dU_e/dx, tangential velocity gradient at the stagnation point. The subscripts are as follows: e, boundary layer edge conditions; w, wall conditions; t, total conditions; and D, dissociation. The heat transfer to a two-dimensional leading edge will be lower than that calculated by Equation 1 by a factor of $\sqrt{2}$. For a spherical or cylindrical leading edge, the velocity gradient at the stagnation point can be found from:

$$\left(\frac{dU_e}{dx} \right) = \frac{1}{R_n} \sqrt{\frac{2(P_e - P_0)}{\rho_e}} \quad (2)$$

where R_n, radius of curvature at the stagnation point; P, pressure, and subscript 0 refers to freestream conditions. For the results presented herein, the assumption $Le = 1$ was made and the boundary layer edge conditions were calculated by solving the equations for a normal shock with subsequent isentropic compression to the stagnation point assuming air in chemical equilibrium.

The upper limit of the resulting surface temperature can be calculated assuming the aerodynamic heating is balanced by the radiative cooling, $\dot{q}_{rad}$, from the surface:

$$\dot{q}_{rad} = \varepsilon \sigma T_w^4 \quad (3)$$

where ε, emissivity; σ, Stefan-Boltzmann constant; and T_w, wall temperature. Setting $\dot{q}_w = \dot{q}_{rad}$ together with an equilibrium air equation of state, one can solve for the wall temperature that balances aerodynamic heating and radiative cooling. This "radiation equilibrium wall temperature" represents an upper limit to the wall temperature since conduction of heat through the leading edge is neglected.

The radiative equilibrium wall temperature was calculated for a $R_n = 2.54$-cm spherical nosetip and a $R_c = 0.254$-cm cylindrical cowl leading edge and the results are presented in Figs 2 and 3. Results are shown for emissivities of 0.5 and 1.0 and flight dynamic pressures between 0.24 and 0.95-atm. Also shown in the

TABLE I Sample engine design characteristics

Component	Mach 6 engine	Mach 10 engine	Mach 15 engine
Inlet			
Efficiency(η_{KE})	0.97	.97	.97
Contraction ratio	6	16.7	25
Combustor			
Efficiency (η_C)	.95	.95	.95
Area ratio (A_{CE}/A_{CI})	2.0	1.5	1.5
Wall area (A_W/A_{CI})	20	20	20
Fuel	JP-7	H_2	H_2
Nozzle			
Efficiency (η_N)	.98	.98	.98
Area ratio (A_{ex}, A_0)	2.0	1.8	1.8

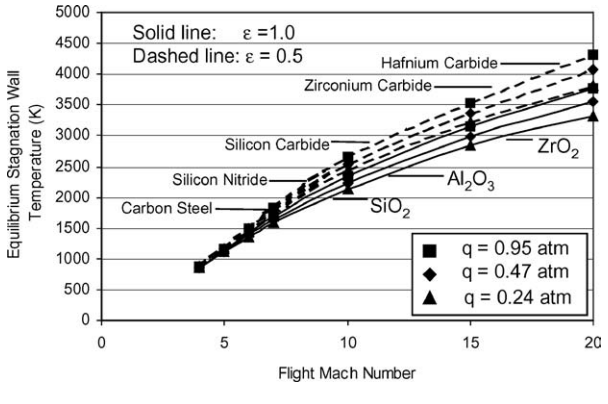

Figure 2 Radiation equilibrium wall temperature at the stagnation point of a 2.54-cm radius nose.

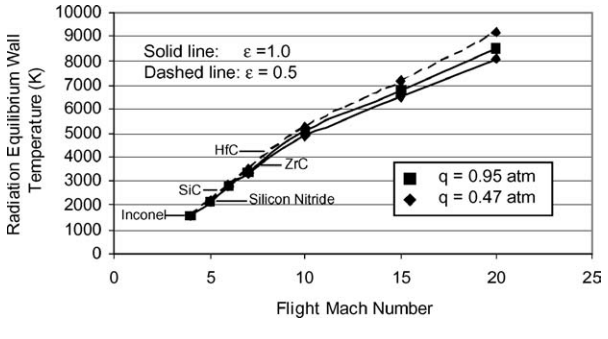

Figure 3 Radiation equilibrium wall temperature at stagnation point of 2.54 mm cowl leading edge.

figure is the melting temperature of selected materials. The stagnation point wall temperature increases with increasing velocity, increasing dynamic pressure, and decreasing emissivity. For a limit temperature of 2000 K at the vehicle nose, the maximum speed of the flight vehicle is in the range of Mach 8 to 10 depending on the altitude and emissivity of the surface. With the sharper cowl radius, the stagnation point wall temperatures are significantly higher with 2000 K temperatures reached at approximately Mach 5 conditions.

2.2. Inlet ramp conditions

The flowfields over a sample three-shock inlet with flow turning angles of 3.6°, 4.2°, and 4.7° were evaluated at Mach numbers between 4 and 10 and a dynamic pressure of 0.47-atm. The flowfields were calculated using a Parabolized Navier-Stokes (PNS) code [5] treating the air as either a perfect gas or a mixture in chemical equilibrium with boundary layer transition assumed to occur at the intersection of the 3.6° and 4.2° ramps. With a specified wall temperature of 833.3 K, the pressure ratio, P/P_0, skin friction coefficient, C_F, and Stanton Number, C'_H, on the inlet third ramp are shown in Fig. 4, where C'_H is defined as:

$$C'_H = \frac{\dot{q}_w}{\rho_0 U_0 (h_{t0} - h_w)} \tag{4}$$

The conversion between C'_H and the more conventional C_H is as follows:

$$C_H = \frac{\dot{q}_w}{\rho_0 U_0 (h_{aw} - h_w)} = C'_H \left(\frac{h_{aw}/h_0 - h_w/h_0}{h_{t0}/h_0 - h_w/h_0} \right) \tag{5}$$

where

$$h_{aw} = h_e + r\frac{U_e^2}{2} \tag{6}$$

The local aerodynamic heating can then be determined as follows:

$$\dot{q}_w = C_H \rho_0 U_0 (h_{aw} - h_w) \tag{7}$$

By balancing the aerodynamic heat transfer with the radiative cooling, the radiation equilibrium wall temperature was calculated assuming unobstructed radiation to free space (i.e., the potential shrouding effects of the engine was neglected). In Fig. 5 the radiation equilibrium wall temperatures are shown for flight at dynamic pressures of 0.47 and 0.95-atm and emissivities of 0.5 and 1.0. The results show wall temperatures significantly below the stagnation point wall temperatures with temperatures below 2000 K for conditions up to Mach 10 flight speeds.

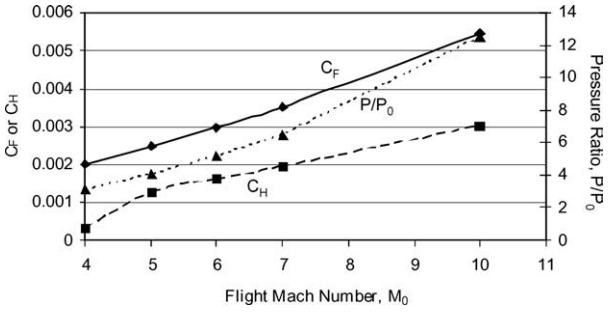

Figure 4 Surface properties on third inlet ramp.

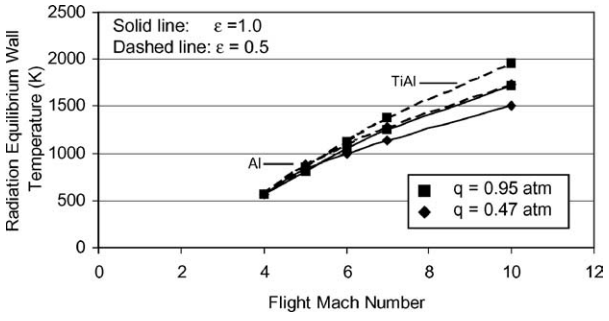

Figure 5 Radiation equilibrium wall temperature on third inlet ramp.

2.3. Upper surface conditions

The operating requirements on the upper surface of a vehicle were estimated at a point 3-m downstream of the leading edge with a local flow-turning angle of 5° assumed. The edge conditions were estimated using the tangent-wedge technique with the skin friction and heat transfer derived using the reference temperature technique [3, 6]. For turbulent flow over the upper surface, the skin friction coefficient was determined as follows:

$$C_f = \frac{0.0592}{(\mathrm{Re}_x^*)^{0.2}} \tag{8}$$

where the Reynolds number is evaluated at the reference temperature, T^*, determined as follows:

$$\frac{T^*}{T_e} = 1 + 0.032M_e^2 + 0.59\left(\frac{T_w}{T_e} - 1\right) \tag{9}$$

The local heat transfer is then determined through application of Reynolds analogy:

$$C_H = \frac{C_F}{2} \tag{10}$$

The local pressure ratio, C_F and C_H are shown in Fig. 6 for the flight speeds between Mach 4 and 20

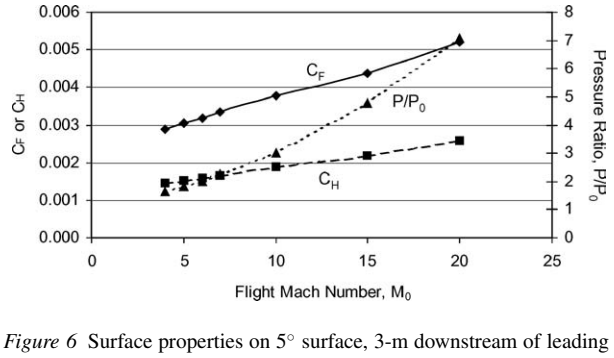

Figure 6 Surface properties on 5° surface, 3-m downstream of leading edge.

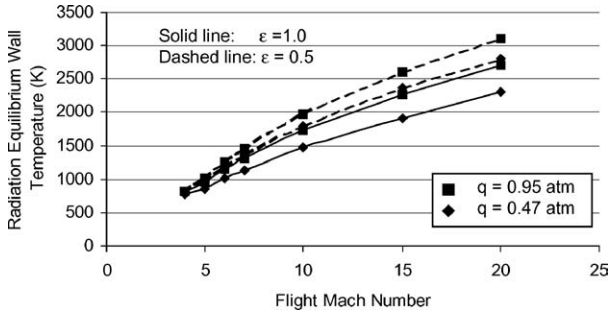

Figure 7 Radiation equilibrium wall temperature 3-m downstream of a leading edge of a 5° ramp.

at a dynamic pressure of 0.47-atm. The pressure ratio increases roughly proportional to the Mach number squared, while C_F and C_H increase nearly linearly with increasing flight Mach number due to a decreasing Reynolds number.

The radiative equilibrium wall temperature for the upper surface is shown in Fig. 7 for flight speeds between Mach 4 and 20, flight dynamic pressures of 0.47 and 0.95 atm, and emissivities of 0.5 and 1.0. Again, the equilibrium surface temperature increases with increasing flight speed, increasing dynamic pressure, and decreasing emissivity. Upper surface equilibrium temperatures are seen to reach 2000 K at speeds between Mach 10 and 15 depending on the trajectory and surface emissivity.

2.4. Internal engine components

The internal engine components are fundamentally different from the external components in that radiation cooling is not available for lowering the wall temperatures. Thus, the engine surfaces must be designed to either handle the recovery temperature of the flow or be cooled to an acceptable temperature.

Engine cycle calculations were conducted for the three sample engines at a flight dynamic pressure of 0.47-atm. Pressures through the sample engines are shown in Fig. 8. Results are provided for the pressure at the end of the inlet compression, P_{ci}, the maximum pressure in the combustor, P_{max}, and the pressure at the end of the combustion process, P_{ce}. The pressures achieved within the engines are generally below 4-atm,

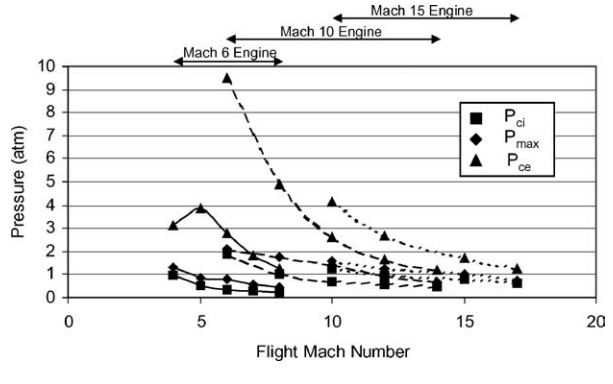

Figure 8 Combustor inlet, maximum and exit pressures in sample engines.

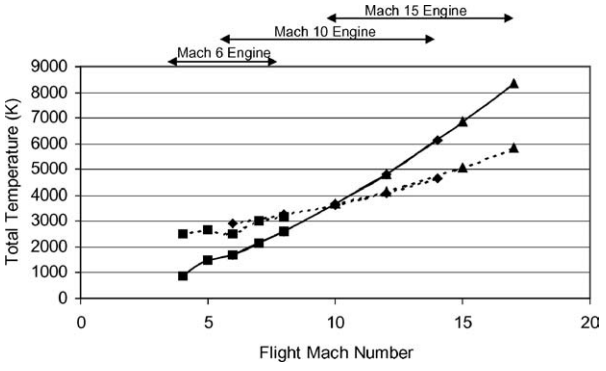

Figure 9 Combustor inlet (solid line) and exit (dashed line) total temperatures in sample engines.

with the exception being the Mach 10 engine operated at low Mach numbers where the effective engine contract ratio is high.

Total temperatures through the sample engines are shown in Fig. 9. Results are presented for both the temperature at the end of the inlet, T_{ci}, and the end of the combustor, T_{ce}. For flight speeds below Mach 10, the total temperature entering the inlet is lower than the combustor exit temperature, but this trend changes at high Mach numbers where the fuel "cools" the flowstream. For the Mach 6 engines, the combustor exit temperatures remain below 2600 K for speeds up to Mach 6 allowing development of uncooled engine structures for expendable systems. For flight speeds above Mach 6, the combustion total temperature is sufficiently high that cooled structures must be developed.

Sample species mass fractions for the combustion products are shown in Fig. 10 for the three sample engines. In each case, oxygen is present due to both the equilibrium combustion mixture and due to the assumption of a combustion inefficiency, which is treated by freezing a portion of the oxygen from the combustion process. The major constituents present are the main combustion products N_2, H_2O, and CO_2. Trace species such as OH, H, and O are present in small quantities. The material used within the engine must resist attack from these combustion products. In addition, cooled engine structures must also accommodate strong thermal stresses and chemical attack by the fuel or its constituents if an endothermic fuel is used.

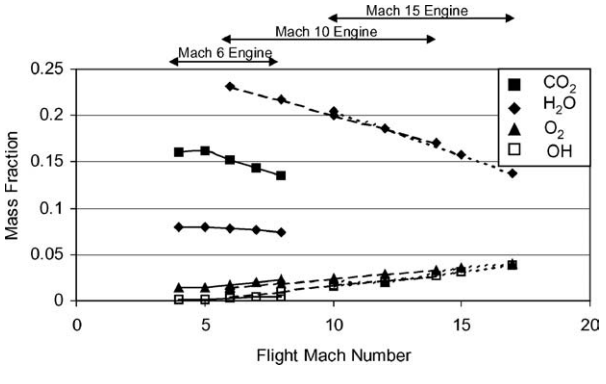

Figure 10 Species distribution at combustor exit of sample engines.

3. Additional considerations

Often in the conceptual or early design phases of missile development, the loads/environments/requirements induced by "non-operational" phases of the mission are overlooked or underestimated. These loads include those due to transportation and storage, insensitive munition considerations, launch effects, and environmental conditions. The magnitude and duration of either individual or combined loads can lead to instantaneous or cumulative damage of components, thus precipitating premature failure when operational loads are applied. In some cases, the magnitude of the loads induced by "non-operational" phases can drive the structural design, materials selection, and resulting performance of the component and entire system. The following paragraphs describe in more detail the considerations and critical issues associated with the non-operational service life of the vehicle/missile.

3.1. Transportation loads

These loads commonly fall into the category of PSH&T (packaging, shipping, handling, and transportation) and encompass the range of conditions introduced to the system during transport from the storage depot to installation on the end-user's weapon platform [7]. Within this category, the most common structural-based loads arise as a result of vibration, shock, and drop conditions. In the case of a missile, packaging (i.e., protective crating) prior to operation provides an effective means to significantly reduce the impact of these conditions as well as the mode of transportation (ground, sea, or air). Packaging can range from simplistic wooden shipping crates to more exotic metallic versions that incorporate hermetic seals to eliminate acidic-based contamination and salt-air moisture sources.

3.2. Insensitive Munitions (IM) requirements

IM requirements are driven by the need to balance weapon system performance with platform survivability, storage, and transport. These requirements influence component-level design issues such as material selection. For a given system, external stimuli guidelines are established that combine the volatility of the booster and air-breathing propulsion fuel systems and warheads in order to determine the potential to generate catastrophic reactions [8]. The environments of concern must be addressed based on missions of interest and handling procedures at the system level (i.e., ship launched, aircraft launched). These environments can be simulated using a variety of representative tests (which may vary from one nation to another) and are covered by various guiding documents (i.e., MIL-STD-2105B, STANAG 4439, UN Orange Book, etc.). Some major representative environments and tests are listed in Table II.

TABLE II Insensitive munition tests and pass criteria

Environment	Test	Pass criteria
External	Fast cook-off	No reaction more severe than burning
High temperature	Slow cook-off	No reaction more severe than burning
Nearby explosion	Sympathetic detonation	No detonation
Impact	Bullet impact	No reaction more severe than burning
	Fragment impact	No reaction more severe than burning
	Shaped charge jet	No detonation
	Spall	No sustained burning
	Drop	No reaction
EMI, lightning strike	Electrical discharge	No reaction

3.3. Launch requirements

The envisioned launch environments for hypersonic missiles have included ship (tube launched), ground-based (tube or transporter launched), and aircraft (wing captive carry with rail or eject launch) weapon platforms. The loads and requirements induced by these launch platforms are vastly different as are the associated launch sequence of events. For tube-launched configurations, the launch event includes egress from the launch tube (including cover contact and push through), booster operation up to air-breathing propulsion system take-over velocities, booster separation, and air-breathing propulsion system operation. For aircraft launched configurations, the aircraft wing captive carry, aircraft eject/rail launch, booster motor operation to take-over velocities, booster separation, and air-breathing propulsion system operation. In addition, aircraft-launched munitions should not compromise the aircraft's "stealthiness," that is, the aircraft's ability to evade or defeat radar and IR detection systems.

The sequence of events for either of the launch approaches requires the integration and interaction of multiple, complex energetic subsystems. This integration task is often overlooked in the development phase as the entire focus is on vehicle operation during sustained hypersonic flight. While the thermal loads dominate during the higher-speed, powered flight phases, structural loads can be more significant during the launch or acceleration phase of the operation; particularly for missiles during aircraft captive carry and eject. Also, while structural loads during flight maneuvers may be at lower levels than those experienced during launch, the degradation of material strength properties with increasing temperature (due to heating and erosion from aerothermal loading or the propulsion system) must be taken into account to insure that the munition has sufficient structural integrity to perform these maneuvers with an adequate safety margin.

3.4. Environmental conditions

The environmental conditions for operational scenarios include long and short-term environmental exposure, external sources that impart damage to the system, and operational environment conditions. Long-term storage tends to be provided in a more controlled environment such as that found in conditioned bunkers at munition storage depots. Temperature extremes, temperature cycling, and humidity are not major contributors.

However, aging of inert and energetic materials can prove to be problematic as system volatility can increase and system performance can decrease due to chemical degradation, interaction, and/or migration over extended time periods.

Short-term storage is typically associated with field storage and inherently has less stringent control of the surrounding environment. Field storage can include significant exposure to temperature extremes (i.e., −60F in the artic to +160F in the desert), temperature cycling, and exposure to humidity. Similarly, flight conditions can mirror the environments for short-term storage; particularly aircraft captive carry where temperature extremes and cycling are similar in magnitude. In mission scenarios, aircraft stowed thermal environments are rapidly followed by simultaneously applied thermal-structural loads (both instantaneous and cyclic). In these conditions thermal shock (where large gradients can exist within a part) and stress oxidation must be considered.

While the C-C and fiber reinforced ceramics (such as CMC's) substrates are generally stable to thermal shock conditions, carbide coatings are more brittle and are subsequently susceptible to flaking and/or spalling. Significant coefficient of thermal expansion mismatches in combination with residual stresses can make the coating-to-substrate interface weak. Incorporating compliant transition layers can increase robustness (with respect to strength) at the coating interface.

Stress oxidation is a concern for carbide coated C-C materials. During long-term exposure to significant combined thermal-structural loads, large deformations in the component can result in coating microcracking, which can in turn lead to hot gas contact and impingement into the C-C substrate and result in rapid degradation of the system. The potential for microcracking increases as the temperature and loading conditions are increased. For structural loads greater than 50% of the material's ultimate strength, the potential for micro-cracking is highly feasible.

External debris impact can impart physical damage to external structures and thermal protection systems. Debris can take several forms including foreign object debris (from runway debris and dust storms) that impact the external surface with sand-dirt particles and small stones, and high-speed flight through clouds (rain, ice, and sleet depending upon altitude and weather conditions). The level of damage that occurs is highly dependent upon the materials selected as the protective coating and base substrate, and the robustness of the interface between the two elements. Particulate impact (depending upon size, velocity, number/density of impacting particles, and particle density) at high speed has been shown to pit and/or remove external insulation and similarly damage composite materials.

A major concern is the response of materials in the aerothermal environment after suffering impact damage from external sources. Subsequent exposure to aerothermal loads after impact damage can allow external high temperature, velocity gas flow to create an erosive environment such that the high temperature flow may penetrate into the substrate with material degradation progressing rapidly. Additionally, for composite materials impacts can be realized internally in the form of delaminations that show no visible signs. This form of damage can significantly impact structural performance and often remains undetected.

Evaluation of Electromagnetic Environmental Effects (E^3) and the impact on component-missile-launcher performance generally fall into several categories; namely electromagnetic interference (EMI), electromagnetic pulse (EMP), electromagnetic vulnerability (EMV), electrostatic discharge (ESD), electromagnetic radiations to ordnance, personnel, and fuel (HERO, HERP, and HERF), precipitation static (P-Static), and lightning (1). From a materials-component standpoint, EMI and EMP must be addressed during the design. The other EMV, EDS, P-Static, lightning, and HERO, HERP, and HERF can be mitigated at the integrated system level.

In the design of the system, material selection becomes important in establishing the performance of the structures housing guidance and control (G&C) and seeker systems relative to potential interference. Nosecone geometry and material property changes as a function of increasing temperature must be considered in designing transmissive-based systems. These characteristics must be assessed with respect to microwave, radar, IR and visible radiation sources and are greatly different among families of materials (i.e., C-C, CMC, ceramics, etc.) as shown below in Table III.

4. Vehicle integration

The integration of numerous subassemblies into functioning vehicle-missile systems requires an extensive system engineering approach to identify critical risk areas and provide acceptable mitigation paths. The design, analysis, and validation testing (that form the basis of the system engineering approach) of the individual components (that make up these subassemblies) yield only a small fraction of the data necessary to predict the response of the subassemblies and integrated system. The interaction of mating components (interface requirements, dimensional constraints, material compatibility) drives individual component geometries, material selection, and load sharing methodologies. Higher order testing of major subassemblies is required to evaluate subassembly interaction and provide calibrated instrumentation necessary for performance monitoring in flight.

In most hypersonic applications, the introduced thermal loads significantly compound the complexity of already taxing structural requirements for flightweight, low-margin/mass fraction designs. Material systems of interest for flightweight high-temperature hardware include carbon-carbon (C-C) materials coated with ceramics such as SiC, HfC, and ZrC, and ceramic matrix composites (CMC's) such as SiC-SiC, C-SiC, C-HfC, or C-ZrC as the primary candidates as shown in Fig. 11 [9–18]. Some metal alternatives such as refractory metals (Niobium), superalloys (Inconel), and intermetallics (TiAl) also exhibit desirable characteristics such as strength/stiffness at high temperature and high

TABLE III Transmissibility characteristics of advanced materials

Materials	Type of radiation					
	Microwave	Radar	Broad band EMI	Far-IR	Near-IR	Visible
Bare C-C	A	A	A	A	A	A
Coated C-C						
C-C SiC Coating	A	A	A	A	A	A
C-C HfC Coating	A	A	A	A	A	A
C-C ZrC Coating	A	A	A	A	A	A
CMC						
SiC-SiC	T	T	T	A	A	A
C-HfC	A	A	A	A	A	A
C-ZrC	A	A	A	A	A	A
C-SiC	A	A	A	A	A	A
Ceramics						
Fused silica	T	T	T	A	T	T
Alumina	T	T	T	A	A	A
BN	T	T	T	A	A	A
SiN	T	T	T	A	A	A

T—Transmissive.
A—Attenuator.

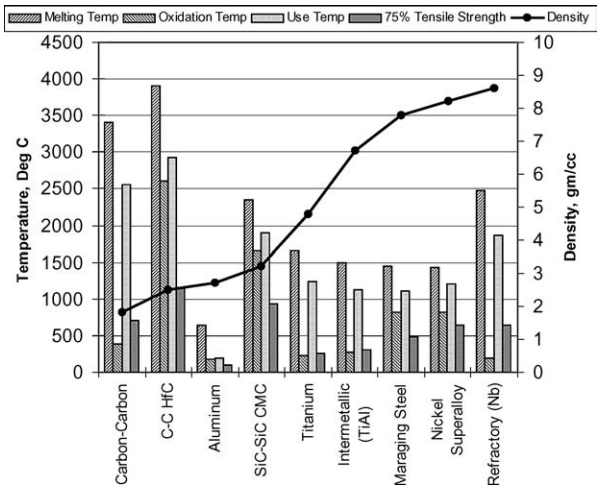

Figure 11 High temperature material characteristics.

melt/oxidation temperature thresholds. However, for higher-speed applications, the component mass penalty associated with increased density tends to make them not viable. The following sections will discuss the issues associated with attachments, seals, and hardware qualification for components manufactured using composite-based coated C-C and CMC materials.

4.1. Attachments

Attachment of components fabricated using materials with vastly differing material properties continues to be challenging; particularly when the environments include elevated temperatures, large temperature gradients, and simultaneously applied structural loads. Design requirements typically include the attachment of hot-to-hot and hot-to-cold structures/component. Attachments can be internal to a structure (i.e., a multi-materials/layers) or between adjacent components (such as thermal tiles or structural members).

Hot-to-hot structures in hypersonic vehicles may include the connections between components within the combustion regions or between thermal tiles on control surface leading edges. In these regions, peak temperature drives the design and excursions can range from 2500 to 3000 K and 1300 to 1900 K for uncooled combustors and leading edges, respectively. In hot-to-cold structures, thermal gradients drive the design. Connections between inlets and airframe/fuel tank regions are an example of this form of connection.

Attachments can be configured for the C-C and CMC material sets using conventional composite material joining approaches and materials suitable for high temperature-strength applications. These approaches include secondary bonding (including ceramic adhesives and metallic-based brazing), threading, and pinning (with superalloy, C-C, or ceramic pins). Critical issues for the high temperature use of these techniques include mismatches in material stiffness and coefficients of thermal expansion, and mechanical property degradation as a function of temperature. The design of the attachment becomes increasingly more complex when integral seals are required to prevent intrusion by pressurized and/or high velocity gases.

4.2. Seals

The incorporation of seals and sealed surfaces in high temperature environments is particularly challenging to prevent penetration by hot, high pressure/velocity gases. Conventional elastomeric seals such as buna-n and silicone (commonly used in cooler, stagnant regions of rocket motors; maximum service temperature range from 90 to 200°C) are no longer candidates in hot-operating structures. The minimum service temperature must also be taken into account as elastomeric seals may become brittle at low temperatures. Consequently, seals must be manufactured from exotic metallic or ceramic materials. Seal configurations of interest include static seals such as those used in pressurized combustion chambers and dynamic seals such as those employed in moveable control surfaces or inlets.

Static seals include ceramic-based rope seals, ceramic-based adhesives, or metallic-based braze.

Rope seals require the use of a male-female gland system with a groove for seal retention. Adhesive seals can be applied to annular, concentric surfaces or to threaded interfaces. Threaded interfaces are a preferred configuration as the tooth profile provides a torturous gas flow path to minimize leakage. Metallic brazing methods for components with annular, concentric interfaces hold promise. This approach shows promise as a high quality; leak proof seal can be developed. However, mismatches in materials must be assessed to prevent localized failure of the seal or mating components during exposure to combined thermal-structural loads.

Dynamic seals include rope seals, similar in configuration to those used in the static configuration. However, seal design becomes more complex as moving as the male-female surfaces move relative to one another during operation. Compression and resiliency of the seal become critical to maintain seal integrity while preventing seal/control surface binding.

For the static or dynamic seals, the localized C-C or CMC region providing the interface with the seal must be sealed to prevent hot gas penetration. Metallic or carbide surface coatings can be applied to reduce permeability levels of the laminate.

4.3. Design validation testing

The level of testing necessary to establish the acceptability of a design and demonstrate design margin is often reflective of the complexity of the component loading conditions and materials of construction. For high temperature composite materials, each new application effectively yields a new material system. This new material is described by fiber selection and reinforcement angles, fiber/matrix percentages, matrix selection, and repeatability of the process/material quality. Typical test sequences in the proof-of-principle phase of development programs include material response testing, pathfinder units to validate component-level form, fit, and function, integration tests with mating subassembly components, and functionality tests to determine overall system response.

The material response testing can include a combination of coupon-level materials characterization and analog test articles to establish "as-fabricated" properties in highly stressed regions. The maturity of the selected material system and the availability of data within the operating regime will often dictate the level of characterization testing that is necessary. Coated C-C materials tend to use more mature/characterized manufacturing processes with more quantified strength data than CMC's. Consequently, some of the fundamental coupon-level material characterization testing may be omitted for C-C's and replaced by property data generated using calibrated material models. However, the lack of data for CMC's, in combination with the maturity level of the current manufacturing approaches, requires that some level of characterization be conducted.

The next step in the characterization program is the development of analog coupons that capture the inherent variability and anomalies in the structure-material system. These coupons must be designed to replicate multi-dimensional stress fields realized in highly loaded (combined thermal/structural) regions of the component. This form of test incorporates the delivered properties of the material based on the selected manufacturing process, laminate architecture, and component geometry and is recommended for both sets of materials.

Component-level testing (via pathfinder units) enables the fundamental response of the unit to be assessed. This testing typically includes an assessment of form, fit, and function for the individual component. Component-level testing then should progress to more complex, integrated testing of the major subassemblies. These tests enable investigations into load sharing between multiple components and should be performed under representative thermal-structural conditions and are critical in the calibration of high-fidelity models.

The final step in the design validation process includes the demonstration of the functionality of the entire system in a combination of ground and flight-testing. A vital link between the two forms of testing is instrumentation. Instrumentation provides data for model calibration as well as a method to assess the performance of the vehicle in flight where post-test observations of hardware may not be possible. The instrumentation used in ground testing, should be the same that is used for flight-testing so that the designer is able to distinguish between fundamental component and gage responses.

As a program progresses and passes from the proof-of-principle phase and into a full-scale development program, higher fidelity testing is necessary to characterize all aspects of system performance. These tests notionally would include aspects of PSH&T, insensitive munitions (if applicable), environmental, and operability. This phase of the testing is costly (so the design must be firmly established), as multiple units are required in order to establish a statistical database for each performance parameter.

4.4. In-process quality control

The ability to understand the manufacturing process and impact on performance, for a given material-component, is vital in establishing a solid quality assurance program. Manufacturing process control for composite material systems is inherently difficult as raw materials, component build-up processes (including operator skill levels), and processing equipment variables can significantly impact the end product quality and resulting thermal-structural performance. It is critical during the development process to initiate quality assurance practices in order to track the maturation process of the component and fully understand the "as-fabricated" condition of the test articles. Typical in-process quality control includes raw material certification, controlled manufacturing procedures with individual unit inspection documentation, and non-destructive evaluation (NDE) of the end product (and potentially at critical phases of the process).

NDE of composite materials (C-C and CMC included) can include radiographic, ultrasonic, and

thermal imaging techniques. These inspection techniques can be readily tailored to detect potential flaws for a specific component (such as coating debonds, cracks, and delaminations). Radiographic inspection is generally a good screening technique as major flaws can be readily detected. However, when determining whether a component should be accepted or rejected (or what performance levels can be safely attained), higher-fidelity inspections using ultrasonic or thermal imaging are necessary to fully describe the flaw (i.e., dimensions, continuous or intermittent, open or closed, etc.). These techniques are more costly due to equipment overhead costs, and require characterization programs to describe potential flaws and accept/reject criteria.

4.5. Acceptance testing

When fabricating components, some level of proof testing (at nominal operating conditions or some level thereof as defined in the system requirements) and destructive testing of tag-end witness coupons is necessary to determine the predicted performance of the component; irrespective of detected flaws. Structural proof testing of the component is generally performed to establish if major inconsistencies exist in the part and process. Tag-end coupons, removed from the component, can be used to determine repeatability of critical processing parameters and material consistency including strength, fiber/matrix/void content, porosity, etc. Destructive testing of random units within a manufacturing lot is performed to provide a higher-fidelity evaluation of manufacturing process consistency. This form of structural testing is generally performed at load levels higher than nominal (maximum operating conditions plus a factor of safety) to confirm design robustness.

It is critical for acceptance testing to be incorporated in the early phases of the development program. This enables a database to be collected that can provide engineering-based accept/reject criteria for components during the production phase.

5. In-service engineering

In-service engineering of fielded systems encompasses assessment of sponsor-driven mission upgrades and refinements (and the impact on current system design and performance), surveillance monitoring of the inventory, and in-service and out-of-service repair.

5.1. Surveillance monitoring

Surveillance monitoring is performed on the inventory to assess the aging characteristics of the system as well determine potential affects on mission performance. As part of this assessment, mission parameters are revised to reflect current threats and applicability in changing battlefield scenarios. For most C-C and CMC materials, aging effects will be minimal with the exception of long-term creep. Areas of concern will be components assembled with preloads. Periodically, random units must be removed from the inventory, inspected, and then tested to evaluate component-system performance levels.

5.2. In-service repair

In-service repair of fielded components is typically limited to quantifiable surface damage (paint or insulation repair) or replacement of non-functioning electronics. The ability to detect internal component defects is generally not possible in the field. Consequently, the repair of structural members manufactured using high temperature material systems is not feasible.

5.3. Out-of-service repair

Out-of-service repair of fielded components typically involves visibly damaged hardware where the level of damage can obviously impact hardware performance and thus limit mission effectiveness. A thorough inspection of this form of damage (and decision on form of rework) would be performed back at a service depot. The inspection process would most likely involve the disassembly of the system and rework or replacement of the damage component(s) with a new component. Most likely, repair of a damaged C-C or CMC component (delaminations, broken fibers, cracked matrix, etc.) would not be possible if structural integrity is required in the damaged zone.

6. Summary

The operating environment of typical hypersonic vehicles with an emphasis on airbreathing engines have been calculated including typical radiation equilibrium wall temperatures for the vehicle leading edge, cowl lip, external surface, and inlet compression surface. Three sample engines were defined spanning the range of hydrocarbon-fueled Mach 4-8 flight and hydrogen-fueled flight at speeds up to Mach 17. Flow conditions at several locations through the sample engines were calculated to provide initial indications of the flow environment. Additional system considerations such as seals, joints, vehicle integration and in-service engineering were addressed.

Acknowledgement

This paper was prepared under the Independent Research and Development program of The Johns Hopkins University Applied Physics Laboratory.

References

1. J. A. FAY and F. R. RIDDEL, *J. Aeron. Sci.* **25**(2) (1958) 73.
2. E. R. VAN DRIEST, *Jet Propulsion* **26** (1956) 259.
3. J. D. ANDERSON, JR., "Hypersonic and High Temperature Gas Dynamics" (McGraw Hill, New York, 1989).
4. J. J. BERTIN, "Hypersonic Aerothermodynamics" (AIAA Education Series, Washington, 1994).
5. W. J. KRAWCZYK *et al*., AIAA-86-1596, 1986.
6. F. M. WHITE, "Viscous Fluid Flow" (McGraw Hill, New York, 1974).
7. E. J. EICHBLATT, JR., "Test and Evaluation of the Tactical Missile," AIAA Vol. 119, 1989.

8. D. M. CURRY and D. W. JOHNSON, "Orbital Reinforced Carbon/Carbon Design and Flight Experience," Space Shuttle Development Conference, July 1999.
9. W. W. TOKARSKY and R.J. DIEFENDORF, *Polym. Engng. Sci.* **15** (1975) 150.
10. R. W. BARTLETT, *J. Amer. Ceram. Soc.* **51** (1968) 114.
11. R. D. CARRAHAN, *ibid.* **51** (1968) 223.
12. R. F. VOITOVICH and E. A. PUGACH, *Soviet Powder Metall. Metal Ceram.* **12** (1973) 314.
13. V. RAMAN, R. DHAKATE and O.P. BAHL, *J. Mater. Sci. Lett.* **20** (2001) 315.
14. RUIYING LUO, ZHENG YANG and LIEFENG LI, *Carbon* **38** (2001) 2109.
15. J. MINET, F. LANGLAIS, J. M. QUENISSET and R. NASLAIN, *J. Europ. Ceram. Soc.* **5** (1989) 341.
16. L. A. FELDMAN, "High Temperature Creep Effects in Carbon Yarns and Composites," in Proceedings of the 17th Biennial Conference on Carbon-American Carbon Society (1985) p. 393.
17. K. M. PREWO, *J. Mater. Sci.* **21** (1986) 3590.
18. W. D. KINGERY, H. K. BOWN and D. R. UHLMANN, "Introduction to Ceramics" (John Wiley and Sons, New York, 1976).

Received 5 November 2003
and accepted 24 March 2004